# Mixed Lamellar Films: Evolution, Commensurability Effects, and Preferential Defect Formation

**E. Huang, P. Mansky,† and T. P. Russell***

*Polymer Science and Engineering Department, Silvio O. Conte National Center for Polymer Research, University of Massachusetts, Amherst, Massachusetts 01003*

**C. Harrison and P. M. Chaikin**

*Department of Physics, Princeton University, Princeton, New Jersey 08544*

**R. A. Register**

*Department of Chemical Engineering, Princeton University, Princeton, New Jersey 08544*

**C. J. Hawker**

*IBM Almaden Research Center, 650 Harry Road, San Jose, California 95120-6099*

**J. Mays**

*Department of Chemistry, University of Alabama at Birmingham, Birmingham, Alabama 35294-1240*

*Received July 30, 1999; Revised Manuscript Received November 8, 1999*

ABSTRACT: The structure of lamellar poly(styrene-*block*-methyl methacrylate), denoted as P(S-*b*-MMA), diblock copolymer films on neutral poly(styrene-*random*-methyl methacrylate), denoted as P(S-*r*-MMA), brush surfaces was examined as a function of annealing time and film thickness using neutron reflectivity and small-angle neutron scattering. Upon annealing, microphase separation occurs quickly with perpendicular and parallel lamellae emanating from the neutral and air surfaces, respectively. This initial growth is followed by a slow increase in the amount of parallel lamellae with a concurrent decrease in the amount of perpendicular lamellae as the samples are annealed further. After long annealing times, the amounts of perpendicular and parallel lamellae do not change significantly. The mixed lamellar structures show a strong commensurability trend with film thickness having a period equal to that of the natural lamellar period. This is explained through the preferential formation of $s_{1/2}$ disclinations having PS cores which dictate the observed commensurability trend. The preferential formation of these defects was observed by field emission scanning electron microscopy on films predominantly comprised of perpendicular lamellae.

## Introduction

Recently, block copolymer thin films have been studied extensively due to their potential applications as nanolithographic templates,[1] separation membranes,[2] and precursors for quantum electronic arrays.[3] Block copolymers are ideal for these purposes since microphase separation occurs on the tens of nanometer length scale, the size of the domains can be controlled by the molecular weight of the copolymer, morphological control is afforded by the relative volume fractions of the two blocks, block copolymers having a variety of different properties can be synthesized, and films can be prepared easily over large areas.[4]

In thin films, the behavior of block copolymers depends primarily on two factors, interfacial interactions[5−8] and commensurability.[9,10] In most cases, there is a preferential wetting of one block at an interface to minimize interfacial and surface energies. Consequently, a parallel orientation of the domains, i.e., cylinders or lamellae, is induced at the interface and propagates throughout the entire film. Commensurability of the film thickness with the natural block copolymer period also plays a central role in the film structure. Films having thicknesses that are incommensurate with the natural repeat spacing undergo quantization of the film thickness to discrete integer or half-integer values of the repeat spacing for symmetric and antisymmetric wetting cases, respectively. This results in the generation of terraces (i.e., islands and holes) at the polymer/air interface and provides a mechanism by which the natural spacing can be maintained throughout the entire film thickness as shown in Figure 1a,b. Confinement of films between two impenetrable boundaries prohibits terracing, and the block copolymer chains must either stretch or compress, resulting in a deviation from the natural period or a rearrangement of some or all of the domains into a perpendicular orientation.[11−14]

Recently, it has been shown that poly(styrene-*random*-methyl methacrylate), denoted as P(S-*r*-MMA), brush surfaces can be used to finely tune the interactions of a symmetric poly(styrene-*block*-methyl methacrylate), denoted as P(dS-*b*-MMA), block copolymer film with its boundaries, where the "d" indicates that the polystyrene block is perdeuterated.[15] For brush surfaces having a styrene fraction of ∼0.60, the interactions between each of the blocks with the random copolymer surface are balanced so that the surface is nonpreferential or neutral to the two components. As a result, block copolymer films placed on the neutral surfaces do not exhibit preferential wetting, and a perpendicular ori-

† Present address: Symyx Technologies, 3100 Central Expressway, Santa Clara, CA 95051.

10.1021/ma9912711 CCC: $19.00 
Published on Web 12/16/1999

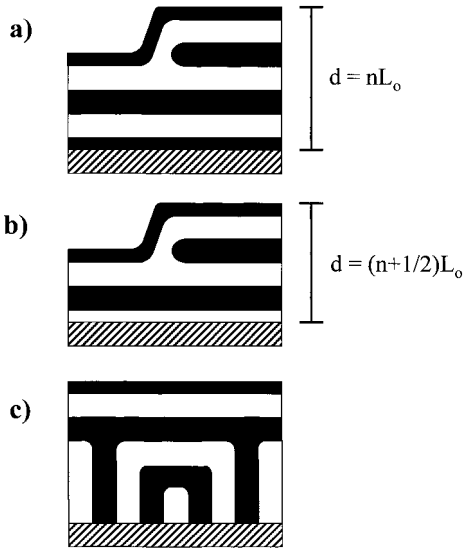


**Figure 1.** Various block copolymer thin film structures: (a) symmetric wetting, (b) antisymmetric wetting, and (c) mixed lamellar structure.

entation of lamellar[16−18]or cylindrical domains[19] with respect to the film boundaries is induced. For lamellar films, complete coverage of the neutral surface with a perpendicular alignment of the lamellae is attained, indicating that this orientation is more favorable than the parallel orientation.[20] At the air interface, however, preferential wetting of the PS block occurs due to its lower surface energy as compared to the case of PMMA. This results in a mixed lamellar structure (Figure 1c) where parallel and perpendicular lamellae are observed at the air and neutral surfaces,[12,21−24] respectively. In strict contrast to the structures induced by commensurability effects, the mixed lamellar structures generated near neutral surfaces form regardless of film thickness as incommensurability of the film thickness with the natural period can be accommodated by either increasing or decreasing the thickness of the perpendicular lamellar region. Consequently, the natural period can be maintained throughout the film thickness without the formation of islands or holes.

In this paper, the mixed lamellar structure of P(dS-*b*-MMA) films placed on neutral P(S-*r*-MMA) surfaces is studied using neutron reflectivity (NR) and small-angle neutron scattering (SANS). First, the evolution of these structures with annealing time will be addressed. Second, the processes by which perpendicular lamellae alleviate incommensurabilities between the film thickness and the natural lamellar period will be examined. Finally, the defects associated with the interface between parallel and perpendicular orientations of lamellae and their relationship to the observed commensurability trends will be discussed.

## Experimental Section

**Sample Preparation.** P(S-*r*-MMA), with a styrene fraction of 0.60 (as determined by NMR), was synthesized in bulk via a TEMPO "living" free radical polymerization using a unimolecular initiator.[15] This provided random copolymers having a hydroxy and TEMPO terminal group. The weight-average molecular weight, $M_w$, and polydispersity, $M_w/M_n$, was measured by size exclusion chromatography to be 9600 and 1.80, respectively. The preparation of the unimolecular initiator[25] and the synthesis of the random copolymer have been described previously.[26]

Random copolymer brush layers were generated by spin-coating films (∼60 nm) of the random copolymer onto clean silicon wafers. The films were annealed under vacuum at 160 °C for 3 days. During annealing, the hydroxy terminal groups attach to the native oxide surface. Subsequently, the samples were thoroughly rinsed with toluene, leaving well-defined brush layers having thicknesses of ∼6 nm, as measured by ellipsometry. The neutral or nonpreferential behavior of these random copolymer surfaces toward PS/PMMA systems has been described thoroughly elsewhere.[15,27]

P(dS-*b*-MMA) was synthesized anionically and Soxhlet extracted in cyclohexane to remove residual polystyrene homopolymer. The "d" indicates that the polystyrene block was perdeuterated. Size exclusion chromatography results yielded $M_w = 50\,000$ with $M_w/M_n = 1.5$. The morphology was observed to be lamellar with a characteristic period of 360 Å and a dPS volume fraction of 0.53 as determined from solution NMR studies. The block copolymer was dissolved in toluene and spin-coated directly onto substrates having the grafted random copolymer brush layer. Films were annealed under vacuum at 170 °C for various times and subsequently quenched to room temperature.

**Characterization.** Neutron reflectivity (NR)[28] and small-angle neutron scattering experiments (SANS) were performed on the NG7 beam guide at National Institute of Standards and Technology in Gaithersburg, MD. For neutron reflectivity, a wavelength of $\lambda = 4.75$ Å was used with a resolution of $\Delta q_z/q_z = 5\%$, where $q_z = (4\pi/\lambda)\sin\theta$ and $\theta$ is the grazing incidence angle. Small-angle scattering was performed using neutrons having a wavelength of $\lambda = 5$ Å ($\Delta\lambda/\lambda = 22\%$), a sample aperture diameter of 0.953 cm, a beam stop diameter of 7.62 cm, and a 2D area detector. Samples were placed directly in the incident beam (silicon is essentially transparent to neutrons) with the angle between the sample surface and incident beam fixed at 90°.

Polymer film etching was performed at the Cornell Nanofabrication Facility (CNF) using a customized reactive ion etcher (RIE) by Applied Materials, Inc. Carbon tetrafluoride, $CF_4$, etching was performed with a gas flow rate of 10 standard cubic centimeters per minute (SCCM), a pressure of less than 1 milliTorr, and a power density of 0.08 W/cm$^2$. These parameters were chosen because low-power, low-pressure $CF_4$-based RIE etches block copolymer films smoothly and at a controllable rate.[17,29−31] The etching rate for the P(dS-*b*-MMA) block copolymer, which reflects an average rate for PS and PMMA, was determined to be 15 nm/min by ellipsometry measurements of the film thicknesses prior to and after etching.

Scanning electron microscope (SEM) images were obtained with a Leo Gemini 982 field emission gun SEM at CNF. To minimize charging, a low incident beam voltage (1−5 kV) was used. Secondary electron signals were collected from both an in-lens and side detector. It has been observed the PMMA etches approximately 3 times faster than PS. Consequently, etching generates topographies in regions having perpendicular lamellae where lighter regions correspond to ridges of PS and the darker regions correspond to troughs where PMMA was etched away. Film thicknesses were measured with a Rudolph Research ellipsometer using a helium−neon laser ($\lambda$ = 632.8 nm) at an incidence angle of 70°.

## Results and Discussion

**Evolution of Mixed Lamellar Film Structures.** A solution of the symmetric P(dS-*b*-MMA) block copolymer in toluene was spin-coated directly onto seven neutral P(S-*r*-MMA) brush surfaces producing films having thicknesses of 150 nm. The samples were annealed at 170 °C under vacuum for 10 min, 30 min, 2 h, 6 h, 12 h, 24 h, and 42 h and subsequently quenched to room temperature. Inspection of the samples showed that all films remained optically smooth, i.e., exhibiting a uniform interference color. This translates into an rms surface roughness of 0.6 nm, as measured by reflectivity.

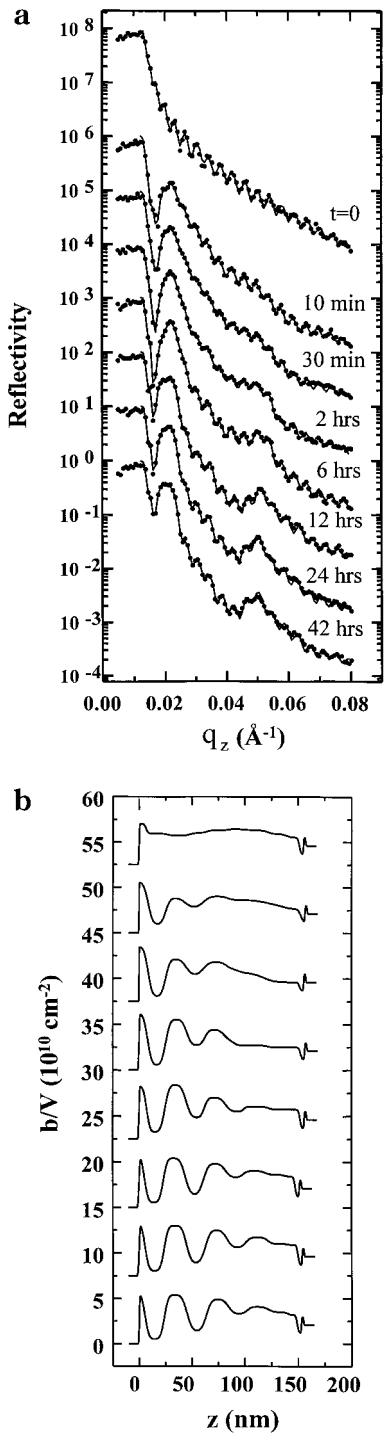


**Figure 2.** (a) Reflectivity data (filled circles) vs $q_z$ as a function of annealing time at 170 °C. The solid lines represent fits to the data. (b) Scattering length density profiles as a function of distance from the polymer/air interface, $z$, obtained from fits to the NR data as a function of annealing time. The data are offset for clarity.

Neutron reflectivity (NR) and small-angle neutron scattering (SANS) experiments were performed on each of these samples to determine the structural evolution. For comparison, one sample was examined with NR and SANS prior to annealing.

The neutron reflectivity data are shown in Figure 2a. The unannealed sample shows a critical edge at $q_z = 0.013$ Å$^{-1}$ and Kiessig fringes characteristic of the film thickness with no other distinguishable features. Upon annealing for 10 min, a first-order Bragg peak at $q_z = 0.022$ Å$^{-1}$ becomes evident, indicating the formation of parallel lamellae. With longer annealing times, the first-order peak becomes larger, and a third-order peak becomes observable at $q_z = 0.050$ Å$^{-1}$. The intensity of the first-order Bragg peak is plotted as a function of annealing time in Figure 3a and clearly shows the formation of parallel lamellae at short anneal times. (The unannealed sample is not represented in the plot.) The amount of parallel lamellae increases with further annealing and levels off at long annealing times.

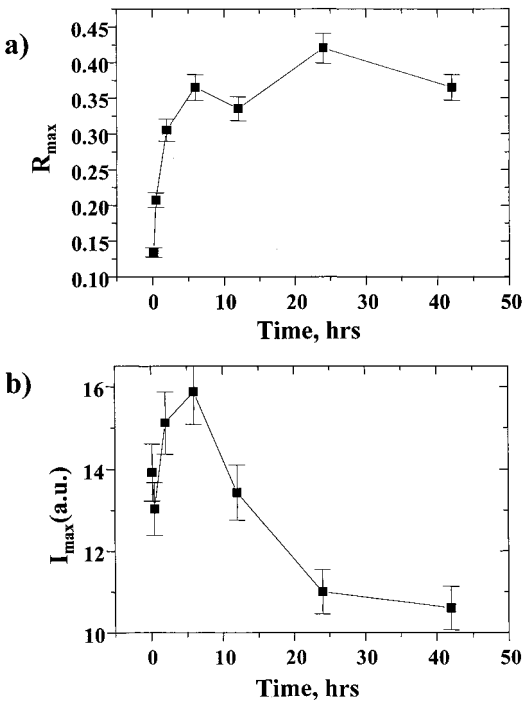


**Figure 3.** (a) Bragg peak reflectivity and (b) maximum circularly averaged SANS intensity as a function of annealing time at 170 °C. The unannealed sample is not represented in these plots.

Fits to the reflectivity data in Figure 2a provide scattering length density, $b/V$, profiles as a function of distance, $z$, from the polymer/air interface for each of the samples (Figure 2b). For the unannealed film, the scattering length density is essentially flat throughout the film. For annealed films, a damped oscillation having a period of ~36 nm emanates from the polymer/air interface. Regions high in scattering length density correspond to dPS, low scattering length densities correspond to PMMA-rich regions, and the random copolymer brush layer is observed at $z = 150$ nm, adjacent to a thin silicon oxide layer ($b/V_{dPS} = 6.37 \times 10^{10}$ cm$^{-2}$, $b/V_{PMMA} = 1.1 \times 10^{10}$ cm$^{-2}$, $b/V_{brush} = 1.25 \times 10^{10}$ cm$^{-2}$, and $b/V_{oxide} = 3.1 \times 10^{10}$ cm$^{-2}$). Complete wetting of polystyrene at the air interface is observed at short anneal times which, consequently, induces the parallel ordering that is damped with increasing distance from the air interface. In contrast, the scattering length density is essentially constant near the neutral random copolymer brush layer ($z = 150$ nm) and corresponds to a region having equal amounts of dPS and PMMA. Since the block copolymer is microphase separated, this suggests that the lamellae at the substrate interface are oriented perpendicular to the neutral random copolymer surface. Thus, the NR results are consistent with a mixed lamellar structure as depicted in Figure 1c.

Small-angle neutron scattering data were obtained at a 90° grazing incidence angle (incident beam is normal to sample surface) for each of these samples. The scattering pattern obtained from the unannealed film did not display well-defined order. For each of the annealed films, however, a scattering ring centered at $q \approx 0.0155$ Å$^{-1}$ is observed, confirming the presence of perpendicular lamellae. The maximum circularly averaged intensity was determined and is plotted as a function of annealing time in Figure 3b. As shown, the scattered intensity is observed to increase initially, diminishes slightly after 6 h, and then does not change significantly after 20 h.

Thus, the NR and SANS results show that upon spin-coating the copolymer film lacks well-defined order as a Bragg peak reflection and a scattering ring are absent. Upon annealing, ordering of the lamellae parallel and perpendicular to the film boundaries occurs very rapidly at the air and neutral random copolymer interfaces, respectively. After 6 h of annealing, the number of perpendicular lamellae decreases while the amount of parallel lamellae increases slightly. This change can be explained by considering the grain growth of the block copolymer domains. The parallel lamellae can be considered as a single grain while the perpendicular lamellae are arranged randomly as many grains. Since parallel and perpendicular lamellae form at the air and substrate interfaces, respectively, minimization of the total amount of grain boundary area leads to growth of the parallel regions of lamellae at the expense of the perpendicular lamellae. After 20 h, the amount of perpendicular and parallel lamellae does not change significantly with further annealing. While it cannot be concluded that an equilibrium state is attained, the mixed lamellar structures are stable even after very long anneal times.

**Commensurability Effects.** As mentioned previously, any incommensurability between the film thickness and natural lamellar period in mixed lamellar films can be alleviated by increasing or decreasing the amount of perpendicular lamellae. Consequently, block copolymer films on neutral surfaces do not exhibit island/hole formation. To investigate this further, a series of block copolymer films of various thicknesses ranging from 50.5 to 156.8 nm were spin-coated onto random copolymer brush layers and annealed for 40 h at 170 °C. NR and SANS experiments were subsequently performed to measure the amount of parallel and perpendicular lamellae with changing film thickness.

Representative NR data and fits are shown for mixed lamellar films of various reduced film thicknesses in Figure 4a. The scattering length density profiles resulting from the fits are shown in Figure 4b. As shown previously, the NR data suggest a mixed lamellar structure with parallel and perpendicular lamellae at the air and substrate interfaces, respectively, for all film thicknesses.

Figure 5 shows the maximum Bragg peak intensity as measured by NR and the maximum circularly averaged SANS intensity as a function of reduced film thickness, $d/L_0$, where $d$ is the film thickness and $L_0$ is the bulk lamellar spacing of 36 nm. NR and SANS data clearly show a periodic behavior, with a periodicity corresponding to $L_0$, superimposed upon a gradual increase in the peak intensities with increasing film thickness. The NR and SANS data are out of phase by exactly $L_0/2$ *w*ith NR and SANS minima occurring at

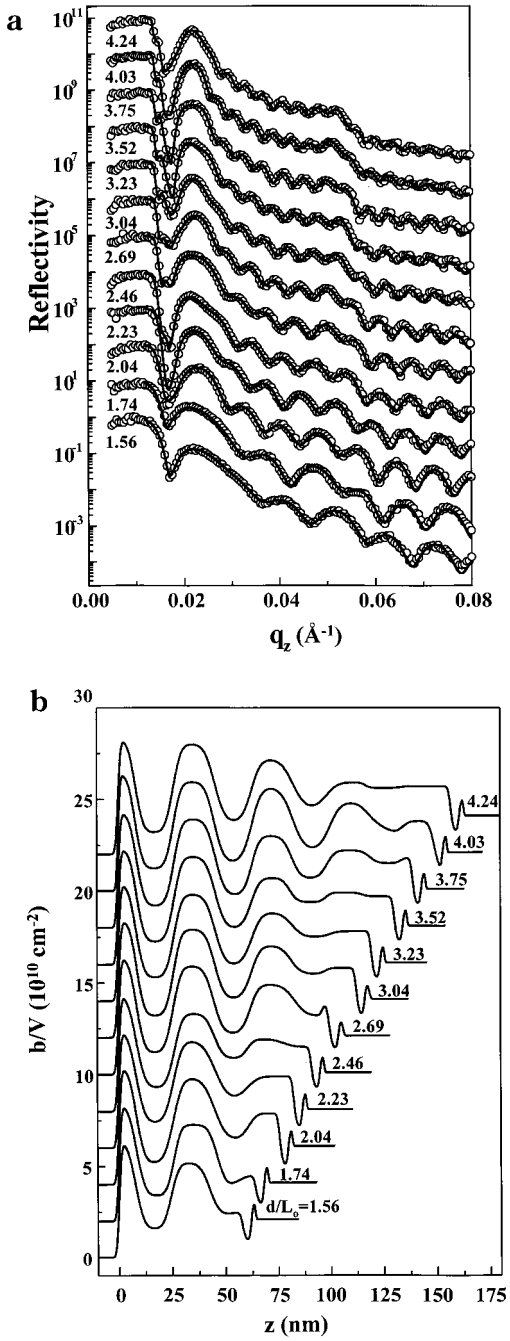


**Figure 4.** (a) Reflectivity data (open circles) and fits (solid lines) vs $q_z$ for films of various reduced film thicknesses, $d/L_o$. b) Scattering length density profiles, as a function of distance away from the polymer/air interface, z, obtained from NR fits for various reduced film thicknesses. The data are offset for clarity.

half-integer and integer reduced film thickness values, respectively. The difference in phase is expected as the sum of the amounts of parallel and perpendicular lamellae in mixed lamellar films must increase linearly with film thickness. The periodicity of $L_0$ is a clear indication of commensurability effects.

**Defect Formation at Perpendicular/Parallel Lamellar Interface.** Diblock copolymers have often been compared to smectic A liquid crystals because there is a mass density wave and a director that can be defined perpendicular to the block copolymer interfaces. Common line and wall defects found in smectic A materials are also observed in block copolymers. A

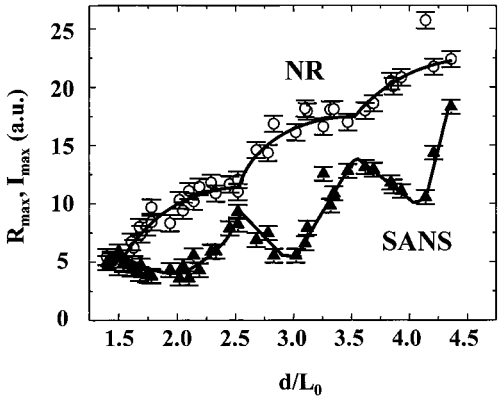


**Figure 5.** Maximum circularly averaged SANS intensity (filled triangles) and Bragg peak reflectivity (open circles) as a function of reduced film thickness.

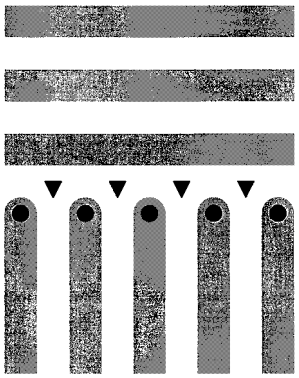

**Figure 6.** Schematic of "T" structure. Triangles and circles mark $s_{-1/2}$ and $s_{1/2}$ disclinations, respectively.

number of studies have addressed various block copolymer defect structures in the bulk[32−38] and to a lesser extent in thin films. Thin film work has been mainly limited to dislocation[39−41] and twist boundary formation[42,43] at the edges of island/hole structures; however, defects not associated with these structures have been addressed to a small extent.[7,30,44]

Misorientation of the two lamellar domains requires the formation of defects at the interface. To understand the commensurability effects observed in these films, the interface between the parallel and perpendicular lamellae and the defects inherent to it must be understood. Perhaps the most related type of defect to those in the mixed lamellar case is the series of "T" junctions observed by Gido et al. in P(S-*b*-I) systems.[34] Matsen also observed these structures in self-consistent field calculations in mixed lamellar films.[24] This type of defect is depicted in Figure 6 and can form when a high asymmetric tilt angle (∼90°) is observed between two lamellar grains. It can also be considered to be a series of two types of disclinations having strengths, $S$, equal to $^1/_2$ and $-^1/_2$. The cores of the two types of disclinations are marked in Figure 6 by the circles and triangles and will be denoted as $s_{1/2}$ and $s_{-1/2}$, respectively. This structure is very similar to the schematic of the mixed lamellar structure as shown in Figure 1c which is also comprised of the two types of disclinations that form at the boundary between parallel and perpendicular lamellae. Despite the fact that the mixed lamellar structure requires bending lamellae around the defect core, this may be more energetically favorable due to the comparatively smaller areal density of disclinations, where lamellar deformation is highest. Consequently, throughout this paper, it will be assumed that the mixed lamellar structures as shown in Figure 1c are characteristic of the observed films.

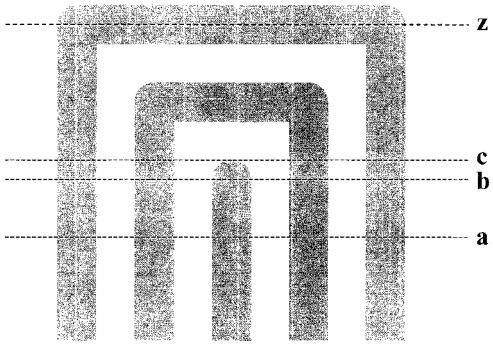


**Figure 7.** Schematic showing the relationship between a $s_{1/2}$ disclination and $d_{\perp,\min}$.

Examination of the mixed lamellar structure in Figure 1c shows that parallel lamellae traverse through the film thickness from the air surface until a $s_{1/2}$ disclination is encountered. Because of this, the significance of the $s_{1/2}$ disclination in mixed lamellar films warrants analysis. Figure 7 shows a schematic of a typical $s_{1/2}$ disclination. In this figure, a mixed lamellar film structure can be described by defining the film boundaries with two parallel lines. If lines *a* and *z* are chosen as the boundaries, the region between lines *a* and *c* are comprised solely of perpendicular lamellae, where line *c* is placed at the end of the $s_{1/2}$ disclination. The distance between lines *a* and *c*, where only perpendicular lamellae are observed, will be referred to as the perpendicular lamellar height and will be denoted by $d_\perp$.

A decrease in film thickness can be modeled by simply moving line *a* closer to *z* (keeping the position of *z* fixed). This effectively decreases $d_\perp$, and consequently, the amount of perpendicular lamellae in the model film is reduced. Line *a* can approach *z*, without affecting the core structure of the disclination, until line *b* is reached. At this point, a further decrease in $d_\perp$ would disrupt the structure of the hemispherical cap that terminates the $s_{1/2}$ disclination core and would therefore be unfavorable. Thus, a mixed lamellar film defined by the lines *b* and *z* would correspond to a film where $d_\perp$ is at a minimum value, i.e., $d_\perp = d_{\perp,\min}$. The minimal perpendicular lamellar height, $d_{\perp,\min}$, would be approximately equal to the radius of the hemispherical cap or $L_0/4$.

As discussed by Chandrasehkar, disclinations and dislocations in smectic A liquid crystals can have different core configurations.[45] For block copolymers, this is also the case, as defects can be distinguished by the composition of the core, which can be comprised of either block component. The energies associated with defects having different cores may differ as influences in the structure of the block copolymer may make one type more favorable. Figure 8a−c shows three series of mixed lamellar structures where the $s_{1/2}$ and $s_{-1/2}$ disclinations exist at the perpendicular/parallel lamellar boundary and alleviate the mismatched alignment of the two different lamellar orientations (PS = light gray, PMMA = black). Each series is comprised of structures having film thicknesses ranging over one lamellar period and differ in the identity of the disclination cores. The disclinations comes in pairs; i.e., for every $s_{1/2}$ disclination there exists one $s_{-1/2}$ disclination. The top schematic, in each series, corresponds to a mixed

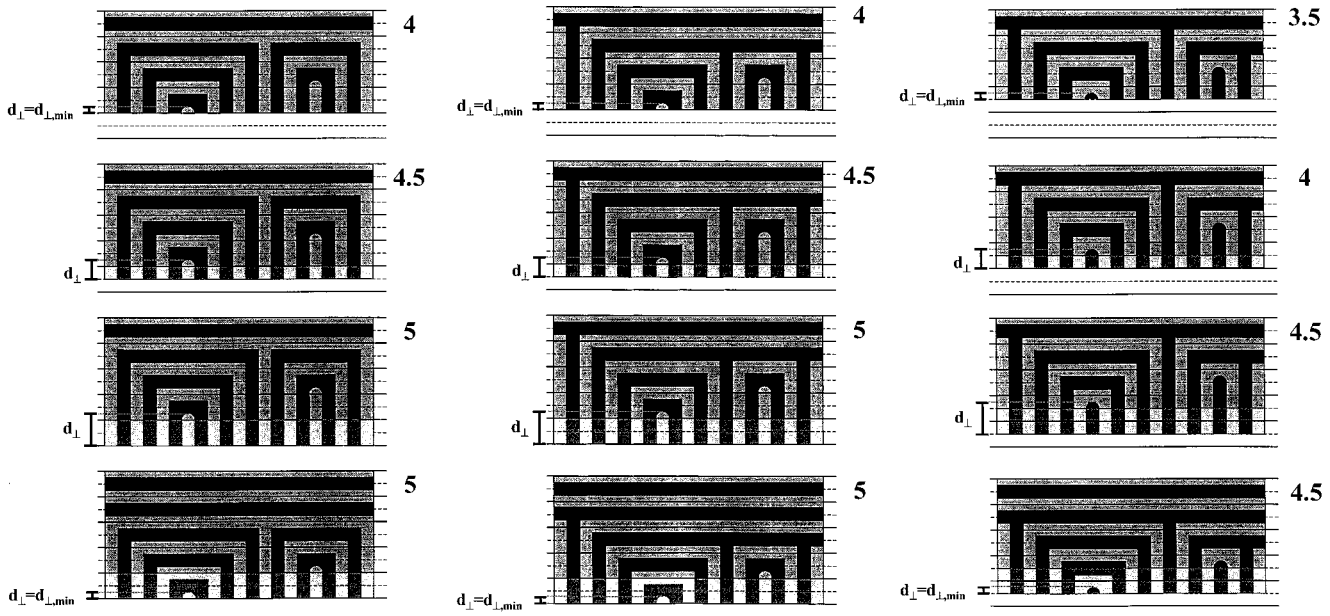


**Figure 8.** Schematics of mixed lamellar structures (PS = light gray, PMMA = black) having (a, left) $s_{-1/2}$ and $s_{1/2}$ disclinations comprised of PS cores, (b, middle) $s_{-1/2}$ and $s_{1/2}$ disclinations comprised of PMMA and PS cores, respectively, and (c, right) $s_{-1/2}$ and $s_{1/2}$ disclinations comprised of PMMA cores. The dark solid lines are spaced at $L_0$, and each schematic is labeled by its reduced film thickness. In each of these series, the film thickness increases until an additional layer of parallel lamellae can be inserted and the perpendicular lamellar height can be minimized, i.e., $d_\perp = d_{\perp,min}$. In (a) and (b), this occurrence is at integer values of reduced film thickness; in (c) this occurrence is at half-integer values of the reduced film thickness.

lamellar morphology where the perpendicular lamellar height is minimized, i.e., $d_\perp = d_{\perp,min} = L_0/4$, while the natural repeat period in the parallel lamellae is maintained. With increasing film thicknesses, the perpendicular lamellar height must increase so that the parallel lamellae maintain the natural period. A point is reached when the perpendicular lamellar height approaches $d_{\perp,min} + L_0$, and at this point, insertion of an additional parallel layer can occur so that the minimal perpendicular height is recovered. Since the total amount of perpendicular lamellae in the film is related to $d_\perp$, films where $d_\perp = d_{\perp,min}$ should necessarily correspond to local minima in the amount of perpendicular lamellae.

In Figure 8a,b, the $s_{1/2}$ core identity is PS while the $s_{-1/2}$ core identity is PS (a) and PMMA (b). In both cases, an additional parallel layer can be inserted (where $d_{\perp,min}$ can be recovered) at integer reduced film thickness values. In Figure 8c, both $s_{1/2}$ and $s_{-1/2}$ have cores comprised of PMMA. In this case, insertion of an additional lamellar layer occurs at half-integer values. From a comparison of the three series, three conclusions can be made. First, the core identity of $s_{-1/2}$ disclination is inconsequential to the behavior of the system as Figure 8a,b shows. Second, the formation of $s_{1/2}$ disclinations having only one type of core leads to a behavior where additional insertion of parallel lamellae occurs periodically with periods of $L_0$. Finally, the film thicknesses for which this occurs is dictated by the core identity of the $s_{1/2}$ disclination. Thus, through this process, commensurability effects are manifested through a periodic variation in the amount of perpendicular and parallel lamellae, where the period is dictated by $L_0$ and the positions in which perpendicular and parallel lamellae are maximized are dictated by $d_\perp$.

Since the NR and SANS data display a commensurability trend having a periodicity of $L_0$ as opposed to $L_0/2$, the mechanism described above does not explain the observed behavior that would be expected for a film having both PS and PMMA $s_{1/2}$ disclinations. However, if $s_{1/2}$ disclinations formed preferentially with PS cores, the commensurability trend would have a period corresponding to $L_0$ and the amounts of perpendicular lamellae would be minimized at integer reduced film thickness values. This is in full accordance with the experimental results.

At this point a reexamination of the scattering length density profiles in Figure 4b is warranted. As shown previously, near the neutral random copolymer brush surface, the scattering length density corresponds to the weighted average of dPS and PMMA and indicates a perpendicular alignment of the lamellae. As the air surface is approached, a periodicity corresponding to parallel lamellae is observed. The interface in which these two regions intersect provides information regarding the defect structure. If only $s_{1/2}$ disclinations having PS cores formed, the first undulation next to the perpendicular lamellae would necessarily correspond to PMMA, and a depression in the scattering length density profile would be expected adjacent to the perpendicular lamellae. Conversely, if $s_{1/2}$ disclinations having PMMA cores formed, the first undulation would correspond to an enrichment of PS, and consequently, an increase in the scattering length density profile would be expected adjacent to the perpendicular lamellar region. However, ambiguities in the scattering length density profiles from the NR data preclude the determination of the component, dPS or PMMA, unequivocally. Nevertheless, better fits were typically obtained for profiles comprised of $s_{1/2}$ disclinations having PS cores.

**Preferential Defect Formation.** Ideally, cross-sectional imaging, i.e., transmission electron microscopy (TEM), could be used to directly examine the defect structures associated with the mixed lamellar films. Normally, samples are prepared by one of two procedures prior to microtoming. First, annealed films can be either floated onto supports[46] or embedded into

matrices[5,47,48] that have mechanical properties similar to the polymer film. Alternatively, films can be cast upon polyimide substrates having a thin evaporated gold layer and then annealed.[49,50] Unfortunately, mixed lamellar structures cannot be generated in a fashion suitable for examination by cross-sectional TEM using either of these approaches. The former procedure is precluded as floating the films off of the random copolymer brush surface is impossible due to adhesion of the block copolymer film to the brush layer. The latter approach is not feasible as the neutral random copolymer cannot be anchored to the thin gold layer; consequently, the mixed lamellar structures cannot be generated on gold surfaces. Substitution of silicon oxide for gold in the latter approach is also not possible, since differences in thermal expansion between the evaporated oxide and polyimide substrate causes substantial cracking in the thin oxide layer upon annealing.[51]

Despite these limitations, the defect structures associated with the block copolymer system used in this study can be closely scrutinized. This is done by using a reactive ion etching/field emission scanning electron microscopy (RIE/FESEM) technique that provides a means by which block copolymer domains oriented perpendicular to the plane of the film and the defects attributed to them can be examined. Although the defects observed in this manner have defect lines that are perpendicular to the film boundaries and, thus, do not directly contribute to the observed commensurability trends, significant information regarding the general formation of defects in this system is obtained and can be applied to the defect structures that are accountable for the observed commensurability trends.

The RIE/FESEM technique is performed by exposing the block copolymer film to a $CF_4$ reactive ion etch and imaging the internal film structure with field emission scanning electron microscopy. It has been found that PMMA etches approximately 3 times faster than PS. As a result, block copolymer domains oriented perpendicular to the film boundaries develop topographies indicative of its morphology and orientation with regions higher in topography corresponding to PS domains which appear bright. By incorporating successive etching and imaging steps, this process can be used to examine the morphology and its orientation at various film depths and has been used to confirm the mixed lamellar morphology in P(S-*b*-MMA) systems on neutral surfaces.

Figure 9 shows a typical FESEM image of the internal structure of a 140 nm block copolymer film confined between two neutral random copolymer surfaces. The observed topography was generated by etching 52 nm of the film away, leaving a film of approximately 88 nm thick. As shown elsewhere, perpendicular lamellae form throughout the thickness of the film in the case where both film boundaries are nonpreferential.[17,18] However, regions lacking in contrast, which can be attributed to parallel lamellae that form due to a lack of registry between perpendicular lamellae emanating from the two neutral boundaries, are observed. Films confined between two neutral surfaces are selected instead of mixed lamellar films for this study as the images obtained from them are ideal for the study of defect structures. Conversely, mixed lamellar structures are mottled due to varying amounts of parallel lamellae across the film surface, and very high defect densities are observed; consequently, difficulty in examining single defects is encountered.

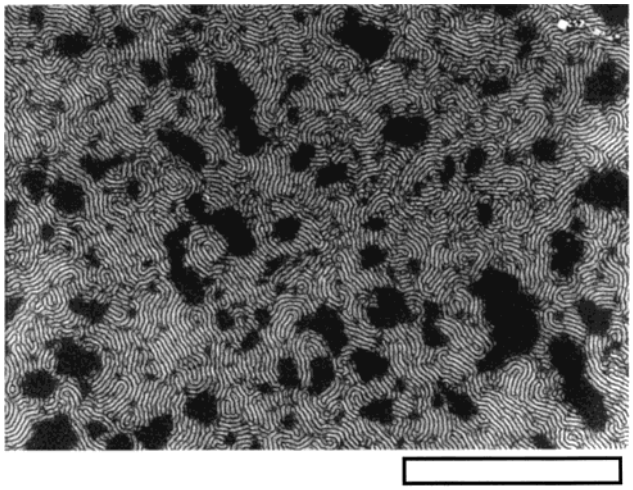

**Figure 9.** FESEM image of film confined between two neutral surfaces after reactive ion etching. Bar = 2 $\mu$m.

Examination of the perpendicular lamellae in Figure 9 shows a number of different types of defects. Three typical line defects, $s_{-1/2}$ disclinations, $s_{1/2}$ disclinations, and edge dislocations, are commonly observed and are shown in Figure 10a−c with the defect cores marked. Interestingly, it was observed that each type of defect was comprised primarily of one type of core. Table 1 illustrates this point where the number and types of defects observed in Figure 9 are tabulated. As the table shows, there is a strong inclination to form $s_{-1/2}$ and $s_{1/2}$ disclinations having PS cores and edge dislocations having PMMA cores. The reason defects form preferentially with one core is not understood and to our knowledge has only been observed in one other case. This was encountered by Liu et al., where edge dislocations attributed to island/hole structures in P(S-*b*-2VP) block copolymer films had cores exclusively comprised of the PVP block.[40]

At the defect core, the conformation of the block copolymer molecules deviates considerably from those observed in unperturbed regions as a substantial interfacial curvature is forced. Two mechanisms can promote interfacial curvature and may, consequently, promote the preferential formation of one type of core. The first involves compositional asymmetry of the block copolymer molecule;[52] i.e., the volume fraction of one block component is slightly larger. As the volume fraction deviates from 0.5, interfacial curvature is promoted with a concavity tending toward the minority component. Thus, defects may form preferentially to minimize chain stretching/compression energies associated with interfacial curvature and space filling requirements. Indeed, Matsen predicted that "T" junction defects in mixed lamellar films can form preferentially with the existence of a slight compositional asymmetry in the block copolymer molecule.[24] The second possible mechanism involves conformational asymmetry[53] of the block copolymer molecule, where one block is effectively stiffer than the other; i.e., the persistence length is larger in one block. This effectively promotes concavity toward block copolymer domains comprised of the stiffer block[54] and may once again lead to a preferential formation of defects.

Consideration of $s_{1/2}$ and $s_{-1/2}$ disclinations observed in this study, which preferentially form with PS cores,

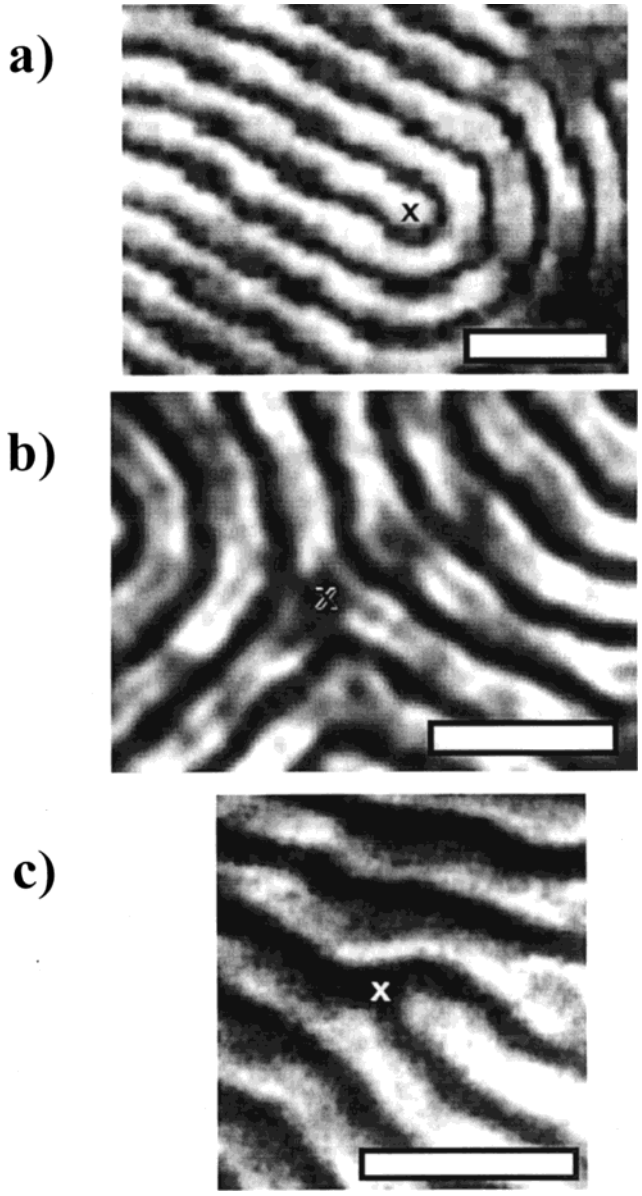


**Figure 10.** FESEM image of a region displaying (a) a $s_{1/2}$ disclination, (b) a $s_{-1/2}$ disclination, and (c) an edge dislocation. Bar = 100 nm.

**Table 1. Defect Statistics on Cores**

| | PS | PMMA |
|---|---|---|
| $s_{-1/2}$ | 365 | 12 |
| $s_{-1/2}$ | 314 | 20 |
| edge dislocations | 35 | 138 |

shows that the two structures display opposite interfacial curvatures near the core. That is, immediate to the core, the interfacial curvature is convex and concave for $s_{1/2}$ and $s_{-1/2}$ disclinations, respectively, with reference to the PS cores. Thus, these results contradict arguments that the preferential formation of defects is based on induced curvatures driven by compositional or conformational asymmetry, and further work on block copolymer defect structures is necessary. Despite this, the preferential formation of $s_{1/2}$ and $s_{-1/2}$ disclinations having PS cores is clearly observed for perpendicular lamellae. An extrapolation of this result to disclinations forming at the interface between parallel and perpendicular lamellae in mixed lamellar films is consistent with the observed commensurability trends.

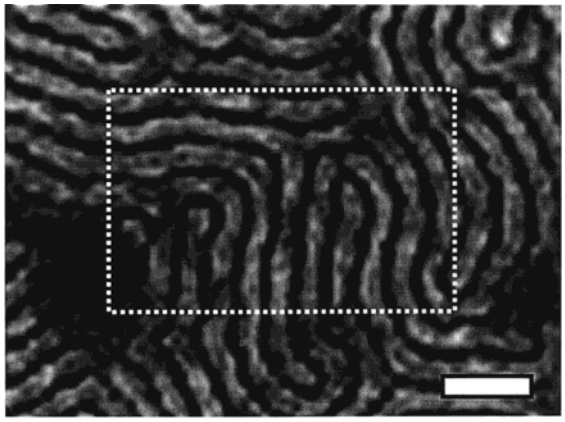

**Figure 11.** Region where lamellae are orthogonal (white box); structure is observed to be similar to proposed mixed lamellar structure. Bar = 100 nm.

Of further note, the preferential formation of $s_{1/2}$ and $s_{-1/2}$ disclinations having PS cores is inconsistent with the "T" structure (Figure 6) as these structures necessitate that the core identity of two disclination types are different. This further supports the premise that mixed lamellar structures such as those shown in Figure 8a are accurate. In fact, Figure 9 shows that, in regions where two lamellar grains are misoriented by 90°, $s_{1/2}$ and $s_{-1/2}$ disclinations form to alleviate the misorientation. As a result, a structure resembling the mixed lamellar structure shown in Figure 8a is generated. An example of such a case is shown in Figure 11.

## Conclusions

Mixed P(S-*b*-MMA) lamellar block copolymer films display structures that are dictated by surface interactions and commensurability effects. At a neutral P(S-*r*-MMA) random copolymer surface, a perpendicular alignment is induced. Conversely, due to segregation of the PS block at the air interface, a parallel alignment is observed at the free surface. Unlike typical block copolymer film structures where the commensurability of the film thickness with the natural period of the block copolymer is manifested through the formation of island/hole structures, mixed lamellar structures do not form islands/holes, and commensurability effects are exhibited as a periodic variation in the amounts of perpendicular and parallel lamellae.

NR and SANS experiments were performed to study the structural evolution of mixed lamellar films. Upon annealing, a parallel and perpendicular orientation of the lamellae are generated at the air and substrate interfaces, respectively. After this initial growth, the amounts of perpendicular lamellae slowly decrease as the number of parallel lamellae increase. At long anneal times, a metastable state is reached where the amounts of perpendicular and parallel lamellae do not change significantly upon further annealing.

The relative amounts of perpendicular and parallel lamellae were found to be highly dependent on film thickness. The period of this behavior corresponded to exactly one lamellar period and is evidence for commensurability effects. Since the interface between the parallel and perpendicular lamellae can be described as a series of $s_{1/2}$ and $s_{-1/2}$ disclinations, schematic mixed lamellar structures having disclinations of varying core types were constructed. From these constructs, the commensurability behavior is found to be dependent

upon the $s_{1/2}$ disclination core identity, and the periodicity observed indicated that $s_{1/2}$ disclinations form preferentially with PS cores.

Indirect evidence for the preferential formation of $s_{1/2}$ disclinations having PS cores was obtained by examining perpendicular lamellae in films confined between two neutral surfaces. In addition to the preferential formation of $s_{1/2}$ disclinations, nearly exclusive formation of edge dislocations having PMMA cores and $s_{-1/2}$ disclinations having PS cores was observed. The reason for this preferential formation is not understood but is consistent with the commensurability trends observed in the mixed lamellar films.

**Acknowledgment.** The authors acknowledge the support of the National Institute of Standards and Technology, U.S. Department of Commerce, in providing the neutron research facilities used in this work and Drs. S. Kline, S. K. Satija, T. Slawecki, and L. Sung for assistance with NR and SANS. This work was supported by the Office of Basic Energy Sciences (DE-FG02-96ER45) and the National Science Foundation through the Materials Research Science and Engineering Center at the University of Massachusetts (DMR-9400488), the Princeton Center for Complex Materials (DMR-9400362 and DMR-9809483), and the Center for Polymeric Interfaces and Macromolecular Assemblies (DMR-9808677).

## References and Notes

(1) Mansky, P.; Chaikin, P.; Thomas, E. *J. Mater. Sci.* **1995**, *30*, 1987.
(2) Martin, C. R. *Science* **1994**, *266*, 1961.
(3) McEuen, P. L. *Science* **1997**, *278*, 1729.
(4) Bates, F. S. *Science* **1991**, *251*, 898.
(5) Hasegawa, H.; Hashimoto, T. *Macromolecules* **1985**, *18*, 589.
(6) Fredrickson, G. H. *Macromolecules* **1987**, *20*, 2535.
(7) Henkee, C.; Thomas, E. L.; Fetters, L. J. *J. Mater. Sci.* **1988**, *23*, 1685.
(8) Anastasiadis, S. H.; Russell, T. P.; Satija, S. K.; Majkrzak, C. F. *J. Chem. Phys.* **1990**, *92*, 5677.
(9) Coulon, G.; Deline, V. R.; Russell, T. P.; Green, P. F. *Macromolecules* **1989**, *22*, 2581.
(10) Anastasiadis, S. H.; Russell, T. P.; Satija, S. K.; Majkrzak, C. F. *Phys. Rev. Lett.* **1989**, *62*, 1852.
(11) Kellogg, G. J.; Walton, D. G.; Mayes, A. M.; Lambooy, P.; Russell, T. P.; Gallagher, P. D.; Satija, S. K. *Phys. Rev. Lett.* **1996**, *76*, 2503.
(12) Walton, D. G.; Kellogg, G. J.; Mayes, A. M.; Lambooy, P.; Russell, T. P. *Macromolecules* **1994**, *27*, 6225.
(13) Koneripalli, N.; Singh, N.; Levicky, R.; Gallagher, P. D.; Satija, S. K. *Macromolecules* **1995**, *28*, 2897.
(14) Koneripalli, N.; Levicky, R.; Bates, F. S. *Langmuir* **1996**, *12*, 6681.
(15) Mansky, P.; Huang, E.; Liu, Y.; Russell, T. P.; Hawker, C. *Science* **1997**, *275*, 1458.
(16) Mansky, P.; Russell, T. P.; Hawker, C. J.; Pitsikalis, M.; Mays, J. *Macromolecules* **1997**, *30*, 6810.
(17) Huang, E.; Russell, T. P.; Harrison, C.; Chaikin, P. M.; Register, R. A.; Hawker, C. J.; Mays, J. *Macromolecules* **1998**, *31*, 7641.
(18) Huang, E.; Rockford, L.; Russell, T. P.; Hawker, C. J. *Nature* **1998**, *395*, 757.
(19) Huang, E.; Russell, T. P.; Harrison, C.; Chaikin, P. M.; Register, R. A.; Hawker, C. J.; Mays, J. Manuscript in preparation.
(20) Pickett, G. T.; Witten, T. A.; Nagel, S. R. *Macromolecules* **1993**, *26*, 3194.
(21) Kikuchi, M.; Binder, K. *J. Chem. Phys.* **1994**, *101*, 3367.
(22) Brown, G.; Chakrabarti, A. *J. Chem. Phys.* **1995**, *102*, 1440.
(23) Pickett, G.; Balazs, A. C. *Macromolecules* **1997**, *30*, 3097.
(24) Matsen, M. W. *J. Chem. Phys.* **1997**, *106*, 7781.
(25) Hawker, C. J.; Barclay, G. G.; Orellana, A.; Dao, J.; Devonport, W. *Macromolecules* **1996**, *29*, 5245.
(26) Hawker, C. J.; Elce, E.; Dao, J.; Volksen, W.; Russell, T. P.; Barclay, G. G. *Macromolecules* **1996**, *29*, 2686.
(27) Mansky, P.; Russell, T. P.; Hawker, C. J.; Mays, J.; Cook, C. C.; Satija, S. K. *Phys. Rev. Lett.* **1997**, *79*, 237.
(28) Russell, T. P. *Mater. Sci. Rep.* **1990**, *5*, 171.
(29) Park, M.; Harrison, C.; Chaikin, P. M.; Register, R. A.; Adamson, D. *Science* **1997**, *276*, 1401.
(30) Harrison, C.; Park, M.; Chaikin, P.; Register, R. A.; Adamson, D. H.; Yao, N. *Macromolecules* **1998**, *31*, 2185.
(31) Harrison, C.; Park, M.; Chaikin, P. M.; Register, R. A.; Adamson, D. H.; Yao, N. *Polymer* **1998**, *1998*, 2733.
(32) Gido, S. P.; Gunther, J.; Thomas, E. L.; Hoffman, D. *Macromolecules* **1993**, *26*, 4506.
(33) Gido, S. P.; Thomas, E. L. *Macromolecules* **1994**, *27*, 849.
(34) Gido, S. P.; Thomas, E. L. *Macromolecules* **1994**, *27*, 6137.
(35) Gido, S. P.; Thomas, E. L. *Macromolecules* **1997**, *30*, 3739.
(36) Amundson, K.; Helfand, E.; Quan, X.; Hudson, S. D.; Smith, S. D. *Macromolecules* **1994**, *27*, 6559.
(37) Amundson, K.; Helfand, E. *Macromolecules* **1993**, *26*, 1324.
(38) Netz, R. R.; Andelman, D.; Schick, M. *Phys. Rev. Lett.* **1997**, *79*, 1058.
(39) Maaloum, M.; Ausserre, D.; Chatenay, D.; Coulon, G. *Phys. Rev. Lett.* **1992**, *68*, 1575.
(40) Liu, Y.; Rafailovich, M. H.; Sokolov, J.; Schwarz, S. A.; Bahal, S. *Macromolecules* **1996**, *29*, 899.
(41) Turner, M. S.; Maaloum, M.; Ausserre, D.; Joanny, J.-F.; Kunz, M. *J. Phys. II* **1994**, *4*, 689.
(42) Carvalho, B. L.; Thomas, E. L. *Phys. Rev. Lett.* **1994**, *73*, 3321.
(43) Carvalho, B. L.; Lescanec, R. L.; Thomas, E. L. *Macromol. Symp.* **1995**, *98*, 1131.
(44) Hahm, J.; Lopes, W. A.; Jaeger, H. M.; Sibener, S. J. *J. Chem. Phys.* **1998**, *109*, 10111.
(45) Chandrasekhar, S. *Liquid Crystals*, 2nd ed.; Cambridge University Press: Cambridge, 1992.
(46) Liu, Y.; Zhao, W.; Zheng, X.; King, A.; Singh, A.; Rafailovich, M. H.; Sokolov, J. *Macromolecules* **1994**, *27*, 4111.
(47) Radzilowski, L. H.; Carvalho, B. L.; Thomas, E. L. *J. Polym. Sci., Part B: Polym. Phys.* **1996**, *34*, 3081.
(48) Shull, K. R.; Winey, K. I.; Thomas, E.; Kramer, E. J. *Macromolecules* **1991**, *24*, 2748.
(49) Kunz, M.; Shull, K. *Polymer* **1993**, *34*, 2427.
(50) Russell, T. P.; Mayes, A. M.; Kunz, M. S. *Ordering Macromol. Syst.* **1994**, 217.
(51) Mayes, A.; Russell, T. P. Unpublished results.
(52) Semenov, A. N. *Sov. Phys. JETP* **1985**, *61*, 733.
(53) Bates, F. S.; Fredrickson, G. H. *Macromolecules* **1994**, *27*, 1065.
(54) Gido, S. P.; Wang, Z.-G. *Macromolecules* **1997**, *30*, 6771.

MA9912711